Broadband measurements of the acoustic backscatter cross section of sand particles in suspension

Cheng He and Alex E. Hay
Department of Physics, Memorial University of Newfoundland, St. John's, Newfoundland A1B 3X7, Canada

(Received 29 July 1992; accepted for publication 15 April 1993)

A method using a broadband transducer to measure the acoustic backscatter cross section of suspended sand particles is investigated. The frequencies used range from 1.3 to 2.8 MHz, and the sand sizes from 100- to 350-μm diameter. The measurements are made in the transducer near field. The measured form factor is compared with the theoretical result for the movable rigid sphere model, and with previous narrow-band measurements.

PACS numbers: 43.30.Ft, 43.30.Ma

INTRODUCTION

The possibility of using ultrasonic pulse-echo techniques for determining the size and concentration of particles in suspensions has been recognized for some time. Applications have included the movement of sediment in rivers,[1] coal slurry transport,[2] and cells in the blood stream.[3] The use of acoustic remote sensing for particle characterization in the ocean was initially directed toward biological scatterers such as zooplankton,[4] and mainly at frequencies of order 10 to 100 kHz. More recently, interest has developed in the acoustic measurement of suspended sediments,[5–13] primarily at frequencies ranging from 100 kHz to several MHz.

A central problem in all acoustical scattering techniques lies in determining the quantitative relationship between backscattered intensity and the concentration of scattering material. The scattering cross section is affected by the size, shape, and composition of the individual scatterers. This makes calculation of the cross section from first principles difficult in general, except for simple shapes. Sand particles are highly irregular. The Reynolds numbers associated with geophysical flows are generally large, certainly for those flows capable of transporting sand in suspension. The problem is, therefore one of remotely characterizing the size and concentration of irregularly shaped particles which assume random orientations in a turbulent medium. A necessary first step is to determine the scattering cross sections of suspended sand empirically, ensemble-averaged over all orientations.

Two experimental methods can be used for ultrasonic determination of scatterer cross sections. The first approach uses many narrow-band transducers, each operating at a different discrete frequency. Alternatively a single transducer of wide bandwidth can be used to increase the information content per pulse in the scattered ultrasound. This method has been used to determine the backscatter cross section of single elastic spheres,[14] using pulses of very short duration and therefore large bandwidth, and of live zooplankton,[15] using chirped transmissions to sweep the transducer bandwidth. One advantage of the broadband approach is that it permits the measurements to be made at higher resolution in frequency than can be readily achieved with narrow-band systems.

The purpose of this paper is to investigate the backscatter cross section of natural sand grains using a broadband transducer. A principal objective of the study was to obtain independent measurements of the sand cross section for comparison with previous narrow-band results.[16] The measurements are made in the transducer near field. This is because in the near field, the transducer beam pattern is approximately nondivergent, and the scattering geometry is therefore similar at all frequencies.

The material is organized as follows. In Sec. I, we outline the relations between the receiver output and scatterer concentration and size. The backscatter cross-section measurements, and comparisons of the results with rigid sphere theory and with previous measurements, are presented in Sec. II.

I. BACKSCATTER FROM SUSPENSIONS

In this section, the relationships between the output voltage of the receiver, and the size, concentration, and backscatter cross section of suspended grains, are briefly summarized. We begin with a discussion of scattering from a single spherical particle. Then scattering from an ensemble of particles in the detected volume is considered. Here, multiple scattering effects will be ignored because we only consider the low concentration case.[16,17]

A. Backscatter from a single particle

At points many wavelengths from the center of the scatterer, the amplitude of the scattered wave takes the form,[18–20]

$$p_s=\frac{p_i a_0 f_\infty(x)}{2z}\,e^{-2\alpha_\omega z}. \tag{1}$$

Here a_0 is the radius of the sphere, $x=ka_0$ is the size/frequency parameter, k is the wave number, α_w is the linear attenuation coefficient in water, and z is the distance from the transducer to observation point (see Fig. 1). The backscatter cross section is proportional to $(|f_\infty(x)|a_0)^2$, where $f_\infty(x)$ is the form factor.

 0001-4966/93/94(4)/2247/8/$6.00

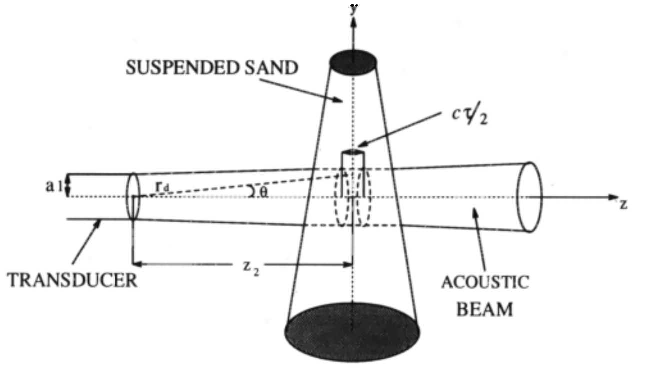

FIG. 1. Scattering geometry.

When the incident wave is a pulse, which may be regarded as a function of time, the incident and scattered pressure pulses have frequency spectra $\Pi_i(\omega)$ and $\Pi_s(\omega)$, respectively, where

$$\Pi(\omega)=\int_{-\infty}^{\infty} p(t)e^{-i\omega t}\,dt. \tag{2}$$

The relationship for each frequency component, in terms of $|f_\infty(ka_0)|$, is obtained by taking the Fourier transform of both sides of Eq. (1). This yields

$$|f_\infty(x)|=\frac{2z}{a_0}\frac{\Pi_s(\omega)}{\Pi_i(\omega)}e^{-2\alpha_\omega z}. \tag{3}$$

B. Backscatter from an ensemble of particles

Now consider the backscattered signal from a cloud of scatterers, where we use the subscript j to refer to individual particles. The total scattered pressure from all scatterers in the ensemble depends on whether a pulsed or continuous wave detection system is used. For typical pulsed detection systems backscattered the mean-square pressure at a specific frequency is given by[6]

$$\langle\Pi_s^2(\omega)\rangle=\frac{\pi}{4}\sum_j \Pi_{sj}(\omega)\Pi_{sj}^*(\omega). \tag{4}$$

Let N be the number of particles per unit volume and $V_d(y,z)$ be the detected volume. From Eqs. (3) and (4), and considering the effect of the transducer directivity $D(y,z,\omega)$, we have the mean-square detected pressure for a cloud of uniformly sized scatterers

$$\langle\Pi_s^2(\omega)\rangle=\frac{\pi}{4}\iint\int_{V_d}\frac{D^4(y,z,\omega)a_0^2|\Pi_i(\omega)|^2|f_\infty(x)|^2}{4z^2}\times e^{-4\alpha_w(\omega)z}N\,dV_d. \tag{5}$$

From Fig. 1,

$$dV_d=2\pi y\,dy\,dz. \tag{6}$$

The receiver output voltage is related to the received pressure at the transducer through an overall system sensitivity constant. Let $v_0(t)$ and $v_i(t)$ be, respectively, the output and input voltage of the instrument which are functions of time t, and $s_t(t)$ and $s_r(t)$ be the overall transmitting and receiving impulse response of the system including both electronics and transducer. The instantaneous incident pressure $p_i(t)$ and instantaneous output voltage $v_0(t)$ of the receiver are, respectively,

$$p_i(t)=v_i(t)*s_t(t), \tag{7}$$

$$v_0(t)=p_s(t)*s_r(t), \tag{8}$$

where the asterisk represents the convolution operation. According to the relationship between the convolution and the Fourier transform, we have

$$\Pi_i(\omega)=V_i(\omega)S_t(\omega) \tag{9}$$

and

$$V_0(\omega)=\Pi_s(\omega)S_r(\omega). \tag{10}$$

The concentration of scatterers in the detected volume is assumed to be uniform. Substituting Eq. (9), Eq. (10), and Eq. (6) into Eq. (5), the square of the output voltage of one frequency component for a cloud of scatterers is

$$V_0^2(\omega)=\frac{\pi S_M^2(\omega)a_0^2|V_i(\omega)|^2|f_\infty(x)|^2}{16}\times\int_{z_2-c\tau/4}^{z_2+c\tau/4}\frac{1}{z^2}\left(\int_0^{a_1}D^4(y,z,\omega)2\pi y\,dy\right)\times e^{-4\alpha_w(\omega)z}N\,dz, \tag{11}$$

where $S_M=S_tS_r$, τ is the duration of the sampling window, and c is the sound speed in the liquid.

The relation between the mass concentration, M, of suspended particles and the number of particles, N, per unit volume can be expressed by

$$M=N\tfrac{4}{3}\pi a_0^3\rho, \tag{12}$$

where ρ is the bulk density of the suspended sand. Then we have

$$V_0^2(\omega)=\frac{3M|V_i(\omega)|^2|f_\infty(x)|^2}{64\rho a_0}|S_M(\omega)|^2A\times\int_{z_2-c\tau/4}^{z_2+c\tau/4}\frac{1}{z^2}\overline{D^4(z,\omega)}e^{-4\alpha_w(\omega)z}\,dz, \tag{13}$$

where A is the transducer surface area and

$$\overline{D^4(z,\omega)}=\frac{2\pi}{A}\int_0^{a_1}D^4(y,z,\omega)y\,dy. \tag{14}$$

We define an overall frequency-dependent system constant $B(z,\omega)$ such that

$$B^2(z,\omega)=\frac{3S_M^2|V_i(\omega)|^2kA}{64}\int_{z_2-c\tau/4}^{z_2+c\tau/4}\frac{1}{z^2}\times\overline{D^4(z,\omega)}e^{-4\alpha_w(\omega)z}dz. \tag{15}$$

We have kept the z dependence in the system constant for convenience, as our measurements are made at fixed z. The output voltage due to the backscattered signal then becomes

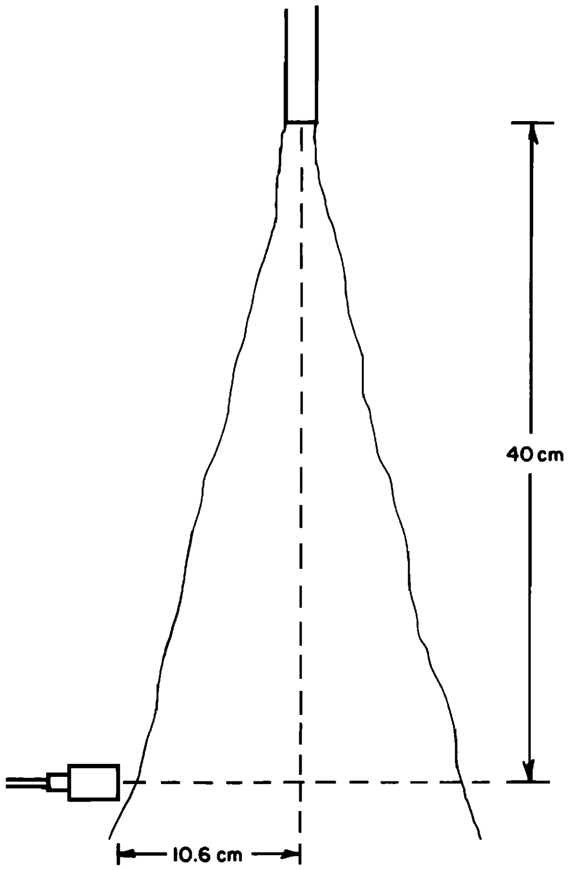

FIG. 2. Sketch of experimental setup for scattering measurements.

$$V_0(\omega)=B(z,\omega)\sqrt{M/\rho x}\,|f_\infty(x)|. \tag{16}$$

It is clear from the above equation that $|f_\infty|$ can be determined from measurements of V_0 provided that the overall system constant is known.

II. BACKSCATTER FROM SAND

A. Experiment design and method description

The scattering experiments were carried out with a high Reynolds number suspended sediment jet. The tank and recirculation system are described elsewhere.[16] The scattering geometry is sketched in Fig. 2. As shown, the acoustic axis intersected the jet centerline at a distance from the nozzle of 40 cm, or about 20-nozzle diameters. For round jets, turbulence is expected to be fully developed at this distance. The width of the jet at the level of the transducer was about 10 cm. The surface of the transducer was 10.6 cm away from the jet centerline. A fine wire suspended from the center of the discharge nozzle was used to align the transducer with the jet axis.

The average concentration distribution across the jet is Gaussian,[10] and can be expressed by

$$M(z-z_2)=M_2\exp[-(z-z_2)^2/2\sigma^2], \tag{17}$$

where z is the horizontal coordinate, and z_2 is the distance from the transducer to the jet centerline. M_2 is the sand concentration at the jet centerline. For our case $\sigma\approx 2.8$ cm.

TABLE I. Size fractions used for form factor measurements. Also listed are midpoints $2a_0$ of size intervals, and the corresponding values of x at 2 MHz.

Size fractions (μm)	$2a_0$ (μm)	$x=ka_0$ (at 2.0 MHz)
106–125	116	0.486
125–150	137	0.574
150–180	165	0.691
180–212	196	0.821
212–250	231	0.968
250–300	275	1.150
300–355	327	1.370
355–425	390	1.634

From Eq. (17), the position where the average concentration decreases by 5% relative to the centerline concentration is 0.9 cm. The width of the region in which the concentration differs by less than 5% of the centerline value is therefore 1.8 cm, which is more than twice our measurement width of 0.75 cm. It should therefore be reasonable to assume that the concentration of suspended sand within the detected volume is uniform on average.

Beach sand was used in the experiments, after being mechanically sieved into the narrow size fractions listed in Table I. To determine the absolute concentration, four 1-l suction samples were taken after each backscatter run using the J tube. The standard error as a percentage of mean of the four samples ranged from 0.24% to 4.45%.

A 0.95-cm-radius commercial broadband transducer was used as the source and receiver. The center, upper (-6 dB), and lower (-6 dB) frequencies of the transducer are 2.09, 2.82, and 1.36 MHz, respectively. Thus the rated bandwidth is around 70% of the center frequency. Figure 3 shows a time series and spectrum of the pulse reflected from an air–water interface. The driving signal, an $O(1\ \mu s)$ pulse, is generated by a Panametrics 5055 PR pulser/receiver. The sampling time is 10 μs which corresponds to a 0.75-cm spatial resolution. Received time-domain signals were acquired with a digital oscilloscope (LeCroy 9400) connected to a personal computer via a GPIB interface. The amplified echo was digitized at a rate of 25 MHz in a time window 10-μs long, centered at a delay corresponding to the range from the transducer to the jet centerline. The fast Fourier transform (FFT) of the 250 acquired points was performed using a Hanning window, and the average of 200 received spectra was calculated. Finally the averaged spectrum was sent to computer to be stored for further processing. The averaged spectrum has frequency resolution of 0.2 MHz, and upper and lower 95% confidence limits are 1.097 and 0.905, respectively. Each run lasted about 1.5 min.

Figure 4(a) and (b) show the backscattered intensities at frequencies from 1.35 to 2.75 MHz, for sand of 180–212-μm diameter at five different concentrations. In these figures, the solid line is the least-squares fit. It can be seen that the measurements are reasonably linear at all frequencies, as expected from Eq. (13).

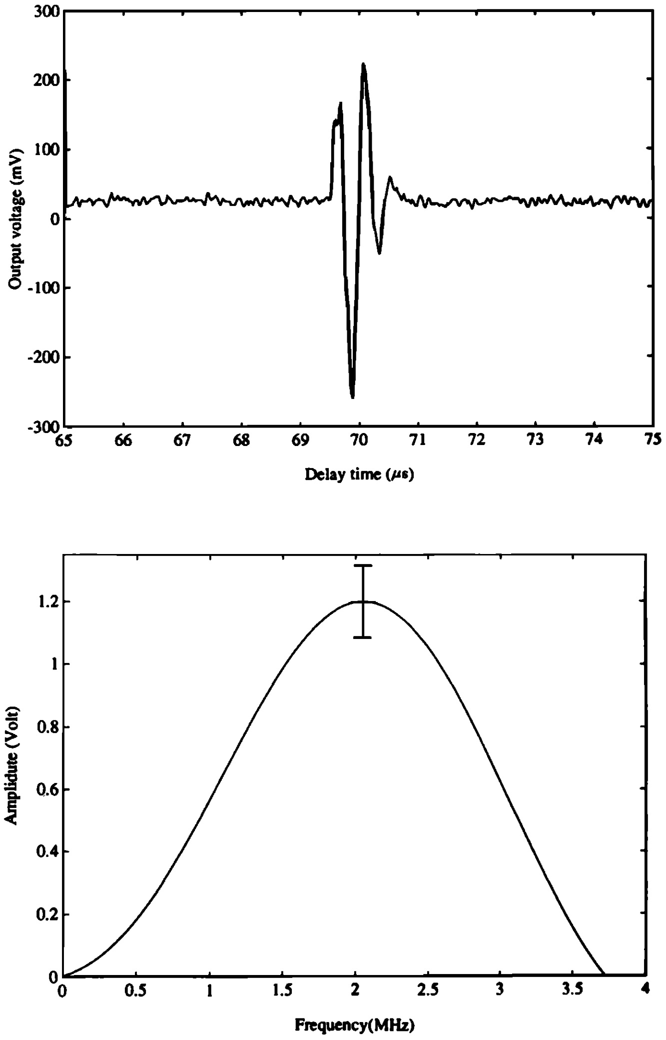

FIG. 3. Time series and spectrum of the pulse reflected from an air–water interface.

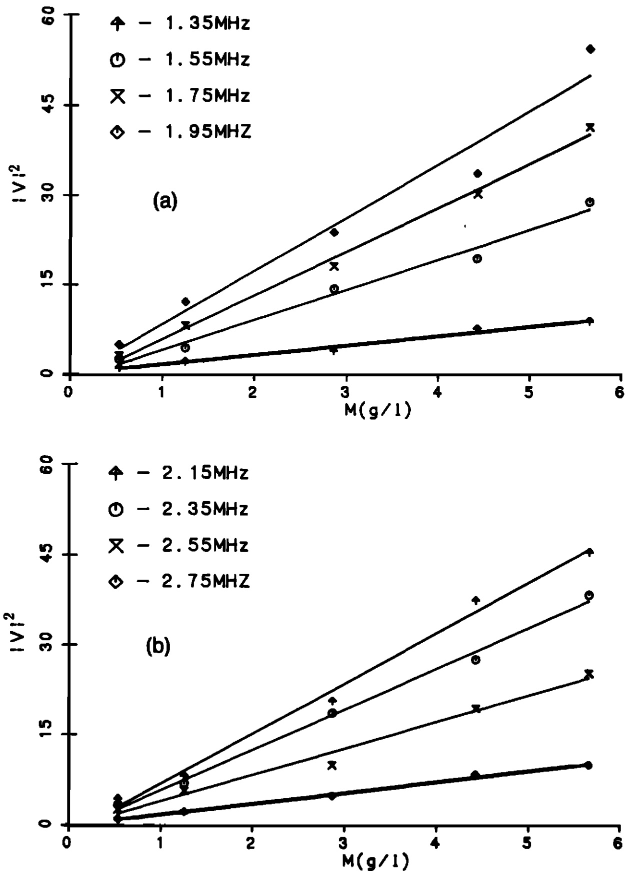

FIG. 4. Squared-mean backscatter (in volt^2) as a function of beach sand concentration at: (a) 1.35 to 1.95 MHz; and (b) 2.15 to 2.75 MHz. Straight lines were obtained by least-squares fit to measured points. Different symbols represent different frequencies, as shown.

B. The system constant

In this section we estimate the overall system constant using the backscatter results for a single grain size, invoking self-reciprocity.[21] Measurements of the form factor made using narrow-band transducers indicate that, in the neighborhood of $ka=1$, the measured values fit the theoretical curve for a rigid movable sphere reasonably well.[16] The idea for determining the system constant from the backscatter measurements is to use the results for a single size chosen such that $ka \approx 1$ at the transducer center frequency, and to obtain B by least-squares fit using Eq. (16) and the form factor calculated from the rigid movable sphere model. These values of B can then be used to determine the form factor for other values of ka using measurements made at different grain sizes.

In our experiments the sand had a narrow but finite-width size distribution instead of being a single size (see Table I). Also, the resolution of the spectra is finite ($\Delta f = 0.2$ MHz). The backscattered signals include contributions from all particle sizes and frequencies in these intervals. So it should be more reasonable to fit the measured results using a smoothed theoretical form factor. The smoothing was done by computing the running average over the interval $\Delta x = \Delta k a_0 + k \Delta a_0$ based on the sand size interval and frequency bandwidth.

Figure 5 shows the results of the fit using the data in

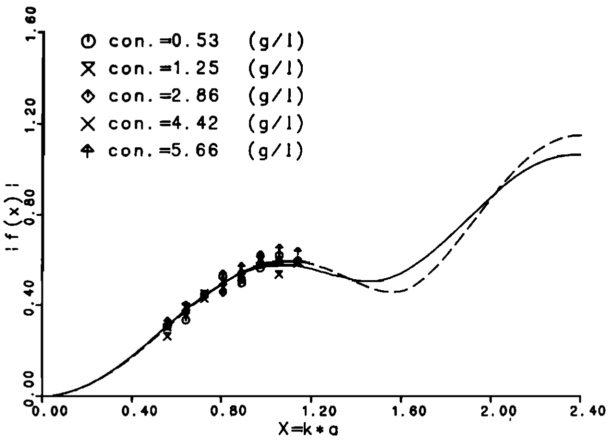

FIG. 5. Backscatter form factor $|f_\infty(x)|$ for 180–212-μm-diameter beach sand. Different symbols represent different concentrations, as shown. The dashed and solid curves represent the unsmoothed and smoothed theoretical results for a rigid movable sphere with the density of quartz.

TABLE II. Averaged overall system constant $\bar{B}$, determined by least-squares fit to backscatter measurements, and B_c determined from reflection measurements. Other parameters are explained in the text.

f (MHz)	1.35	1.55	1.75	1.95	2.15	2.35	2.55	2.75
$\bar{B}$ (mV)	177	244	276	296	276	239	198	135
B_c (mV)	550	800	1050	1150	1200	1100	850	650
B' (mV)	125	192	270	312	338	322	260	203
$\bar{B}/B'$	1.42	1.27	1.02	0.95	0.82	0.74	0.76	0.67
$[\overline{D^4}]^{1/2}/\overline{D^2}$	1.45			1.61				2.04

Fig. 4. The dashed line is the theoretical form factor $|f_\infty(x)|$ for a rigid sphere. The solid curve is the smoothed rigid sphere result used in the fit. The resulting values of $\bar{B}(z,\omega)$ at $z=10.6$ cm, where the overbar denotes the fact that measurements at several concentrations were used to obtain the least-squares estimate at each frequency, are listed in Table II.

C. Form factor

A set of experiments were carried out using three different sizes and six different concentrations for each size (see Table III). The results for $|f_\infty(x)|$, computed using $\bar{B}$ from Table II, are shown in Fig. 6. The precision of these form factor estimates was determined as follows. From Eq. (16) it can be seen that the error in $|f_\infty|$ is due to the error in the system constant B and in the ratio $V_0/\sqrt{M}$. The standard errors in the values of B were estimated from the five separate determinations at each frequency (see Fig. 4), and ranged from 1.4% to 3.2%. Similarly, the standard errors in $V_0/\sqrt{M}$ were estimated from the standard deviation of the six measurements at each frequency, and ranged from 1.3% to 5.5%. The standard error in $|f_\infty|$ was taken to be the square root of the sum of the squares of the errors in B and $V_0/\sqrt{M}$, and is represented by the errors bars in Fig. 6.

These results for $|f_\infty|$ are combined, and plotted as averages at each frequency, in Fig. 7. It is encouraging that the estimated values of $|f_\infty(x)|$ are substantially the same for the three sizes in the regions of overlap. The measured form factors are also in substantial agreement with the theoretical curve for a rigid sphere in the low-frequency/small-size region, $x \leqslant 1$. At higher values of x, the measurements are larger than predicted by rigid sphere theory, although they exhibit similar curvature. We note that this curvature is expected physically, being the result of the motion of the scatterer with respect to its center of mass. (This is evident, for example, from the comparison with the rigid movable and rigid immovable sphere models given in Ref. 16.)

Also shown in Fig. 7 is a dashed curve. This curve represents the narrow-band results,[16] and was obtained by fitting a rational fraction expression to the narrow-band measurements.[22] (The fit to the narrow-band measurements is very good, the rms deviation being less than 6%.) The broadband measurements are well represented by the dashed curve. This indicates that the form factor values determined by broadband backscatter are in substantial agreement with those obtained independently by narrow-band techniques.

The rigid sphere calculations were made for a movable scatterer with the density of quartz. It is of interest to consider the possible effects of the elastic properties of the particles on the form factor in this low ka range. Precise values for the elastic constants of sand grains are not well known, and can be expected to vary with grain mineralogy. Nevertheless, rough estimates can be made from Ref. 27. The elastic constants listed there for granite and sandstone quartzite give compression and shear wave speeds in the range 4800–6200 and 3200–4200 m/s, respectively. These values are not radically different from those used by Hay and Mercer[20] for quartz ($c_p=5100$ m/s, $c_s=3200$ m/s) and aluminum ($c_p=6370$ m/s; $c_s=3120$ m/s). Their calculations of $|f_\infty|$, compared to the dashed line in Figs. 5 and 6, show 10%–20% higher values in the vicinity of the maximum at $ka \approx 2.4$. The differences below $ka=2$ are small. Including elasticity therefore leads to improved agreement with the narrow-band measurements at $ka>2$, but would not significantly affect the present comparison with measurements below $ka \approx 2$.

III. DISCUSSION

As part of this study, reflection measurements from an air–water interface at normal incidence were made to investigate the divergence of the transverse-averaged beam as a function of frequency and distance in the near field. It had also been our intention to use the air–water reflection to determine the system constant. The reflection measurements provided only an approximate check in this respect, however, because of the intrinsic differences in the frequency dependence of the effective directivity for the two types of measurement.

TABLE III. Sizes and centerline concentrations for the form factor measurements. (Temperature=20.9 °C, $c=1484.4$ m/s.)

Size (μm)	$2a_0$ (μm)	M (g/l)					
106–125	115.5	0.355	0.997	2.02	3.32	4.09	4.67
180–212	196.0	0.554	1.15	2.13	3.12	4.27	5.27
300–350	325.0	0.418	1.14	1.99	2.46	3.01	3.75

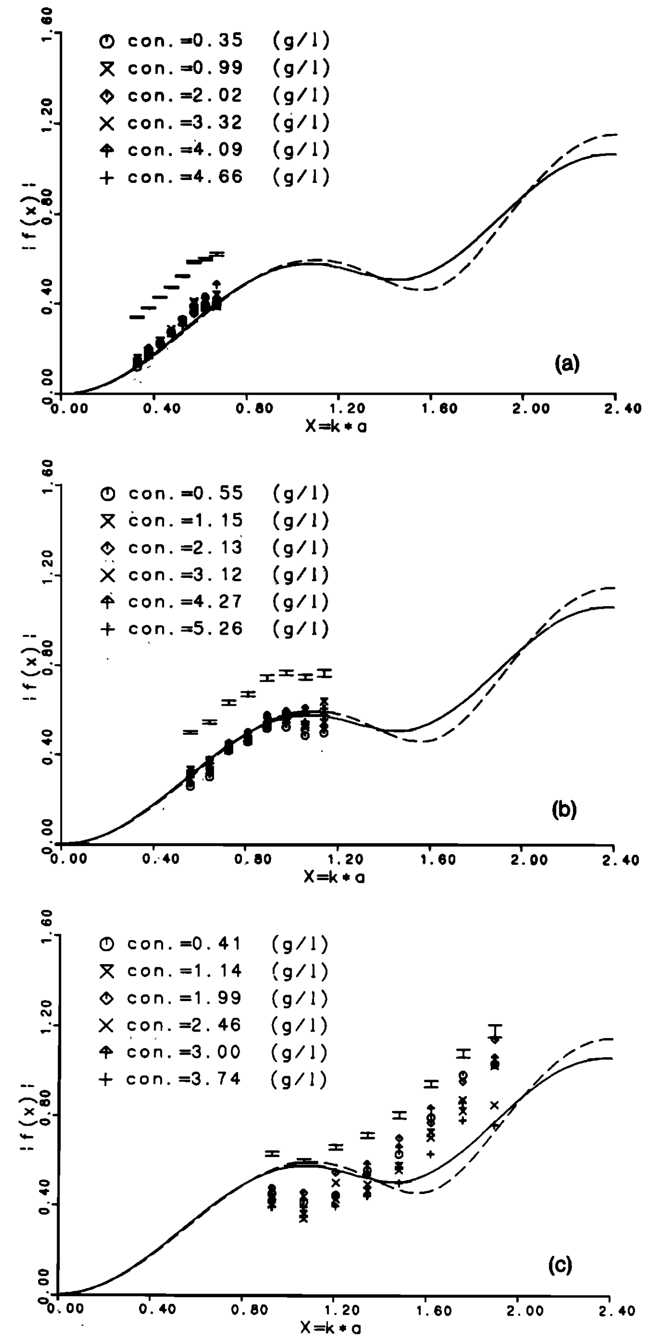

FIG. 6. Backscatter form factor $|f_{\infty}(x)|$ for beach sand: (a) 106–125 μm; (b) 180–212 μm; and (c) 300–350-μm diameter. Dashed and solid curves as in Fig. 5.

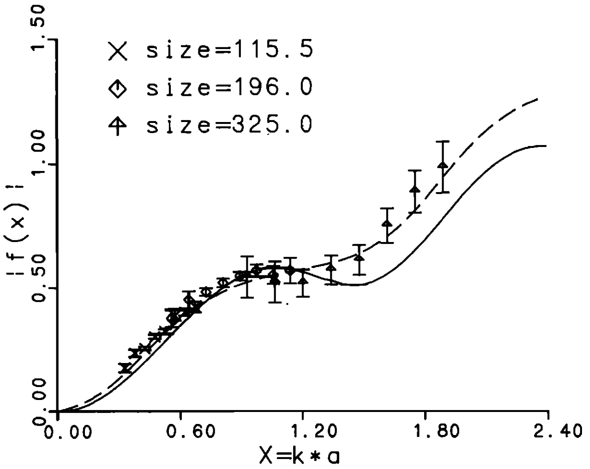

FIG. 7. Backscatter form function $|f_{\infty}(x)|$ for beach sand, showing the mean at each frequency of the multiple concentration measurements for the three size fractions in Fig. 6. Solid curve as in Figs. 5 and 6. Dashed line explained in text. Error bars represent ± 1 standard deviation.

A. Beam divergence

In a monostatic reflection measurement, the on-axis sound pressure received at a distance z_c from the air–water interface is given by

$$p_s(t)=\overline{D^2(2z_c,\omega)}p_iR_{wa}e^{-2\alpha_\omega z_c}, \tag{18}$$

where p_i and p_s are the incident and scattered acoustic pressures, R_{wa} is the air–water plane-wave reflection coefficient, and $\overline{D^2(2z_c,\omega)}$ is the transverse mean-squared directivity,

$$\overline{D^2(z,\omega)}=\frac{2\pi}{A}\int_0^{a_1} D^2(y,z,\omega)y\,dy. \tag{19}$$

Figure 8 shows the results of the reflection measurements, corrected for water attenuation using the expression given by Fisher and Simmons,[23] and normalized by the values at the distance of closest approach to the surface. Calling this distance z_0, the plotted points are a measure of $[\overline{D^2(z,\omega)}/\overline{D^2(z_0,\omega)}]^{1/2}$. The measurements at 2 MHz are compared with theory in Fig. 8(a). Theoretical curves are shown for both uniform (crosses) and nonuniform (dashed) surface vibration, respectively. The nonuniform case corresponds to the first vibrational mode. The details of these computations are given elsewhere,[24] and are based on the near-field formulation of Hasegawa *et al.*[25] It can be seen from the figure that the theoretical curve for uniform surface vibration provides a reasonable fit to the measured results (solid curve). This implies[24] that many vibrational modes are excited by the short duration pulse, as one would expect.

Figure 8(b) shows the measurements at 1.4, 2.0, and 2.8 MHz. The slopes of the measured curves for the three different frequencies are very similar, indicating that the beam divergence is essentially the same over the bandwidth of the transducer. (Recall that this was the reason for making the scattering measurements in the near field.) The beam divergence is also weak, decreasing roughly linearly with distance, and by less than 2% in amplitude in the 10- to 11-cm operating range for the scattering experiments. This indicates that the integral in Eq. (13) could be simplified by setting D=constant.

B. System constant

An overall system constant B_c for the reflection measurement is defined such that

$$B_c=\frac{V_0}{R_{wa}}=\overline{D^2(2z_c,\omega)}S_M(\omega)V_ie^{-2\alpha_\omega z_c}. \tag{20}$$

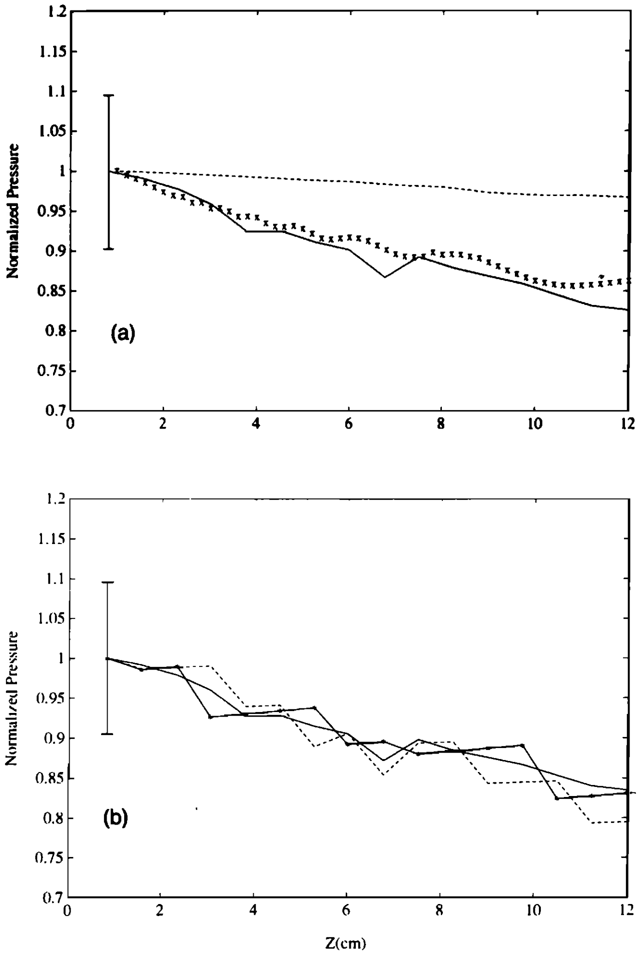

FIG. 8. (a) Normalized amplitudes of the pulse reflected from an air–water interface as a function of distance, at 2.0 MHz. The measurements are shown by the solid curve. The dashed curve and crosses are the calculated results for a nonuniformly and uniformly vibrating piston, respectively. (b) Normalized amplitudes of the reflected pulse at different frequencies: 1.4 MHz (dash), 2.0 MHz (solid), and 2.8 MHz (stars connected by solid line). The error bars represent the 95% confidence limits for the measurement.

Comparing this expression with Eq. (15), it can be seen that for $z=2z_c$, the system constant determined from the reflection measurement will be similar to that for the scattering measurements. The two system constants are not identical, however, and in particular, the frequency dependence is different.

The results for B_c at a distance z_c of 5.3 cm are listed in Table II for $R_{wa}=0.9994$, computed using the usual plane-wave reflection formula.[26] To compare these values for the overall system constant with the data for $\bar{B}$ obtained from the scattering measurements, we take the ratio of Eqs. (15) and (20), with $z_c=z_2/2$, obtaining

$$\frac{B(z_2,\omega)}{B_c(z_2,\omega)}=\frac{[\overline{D^4(z_2,\omega)}]^{1/2}}{\overline{D^2(z_2,\omega)}}\sqrt{\frac{3kAc\tau}{128z_2^2}}, \tag{21}$$

since to a very good approximation $e^{-\alpha_w z_2}=1$ for our measurements. Making the rough assumption initially that the ratio $[\overline{D^4}]^{1/2}/\overline{D^2}$ is independent of frequency and equal to unity, we obtain

$$B'=B_c\sqrt{\frac{3kAc\tau}{128z_2^2}}, \tag{22}$$

where B' is now an approximate estimate of B, obtained from B_c. Table II lists the values of B', calculated using the values of B_c in Table II, and $A=2.85$ cm^2, $c=1496$ m s^{-1}, $\tau=10$ μs, and $z_2=10.6$ cm.

Comparing $\bar{B}$ with B', we find that at frequencies near the 2-MHz center frequency, agreement is reasonably good. The reflection measurements had to be made with a lower (40 dB) receiver gain, because the surface-reflected signal was so much stronger than the backscatter from suspended sand. Perhaps one might have been satisfied with this level of agreement. However, beyond the center frequency the differences approach 30% to 40%, with the reflection estimates being smaller at low frequencies, and larger at high frequencies. Such a consistent trend with frequency begs explanation. The most likely cause appears to be the different frequency dependence of the effective directivity in the two types of measurement. As one measure of this, the computed values of $[\overline{D^4}]^{1/2}/\overline{D^2}$ are listed in Table II for the center frequency and the frequencies at the upper and lower extremes of the bandwidth. Clearly, the ratio of the two measured system constants is sensitive to this term. Differences across the bandwidth of up to 30% relative to the center frequency can result. This cannot be the whole story, however, because the variation of $[\overline{D^4}]^{1/2}/\overline{D^2}$ with frequency is such as to amplify the departures from unity of the ratio $\bar{B}$ with B' listed in Table II. We suggest that the assumption that the near-field cross-sectional area of the beam is equal to the area A of the transducer and independent of frequency is not correct. Furthermore, the effective area of the beam at a given frequency need not be the same for the two types of measurement. In a backscatter measurement, for example, the beam divergence is compensated by the increased number of scatterers insonified. In a specular reflection measurement, diverging rays incident upon the reflecting surface need not impinge upon the transducer surface after reflection. The conclusion is that, for scattering measurements on ensembles of particles in suspension, the effective system constant is most readily determined by using suspensions of standard target particles.

IV. CONCLUSIONS

Measurements of the backscatter form factor of natural sand, made monostatically using a broadband pulse in the transducer near field in the range $0.32\leqslant x\leqslant 1.9$, have been shown to be in substantial agreement with measurements made previously using narrow-band transceivers. As for the previous measurements, the measured form factor follows the theoretical curve for a movable rigid sphere reasonably well in the low-frequency/small-size region ($x\leqslant 1$). For larger x, the measured values are larger than predicted by rigid spherical scatterer theory.

The results presented here are promising, and indicate that it is feasible to determine the scattering cross sections of particles in turbulent suspensions using broadband pulses. A necessary part of making such measurements is the determination of the system constant. We have found that, for the purpose of scattering measurements of particles in suspension in the transducer near field, this constant is most readily determined using standard target particles rather than, for example, the reflection from a pressure-release surface.

ACKNOWLEDGMENTS

We are grateful to Doug Wilson for his help with the measurements, and to Anna Crawford for the function fitting the narrow-band measurements. Rod Campbell provided computational support. This work was funded by a Research Agreement from the Department of Energy, Mines, and Resources of Canada, and an Operating Grant from the Natural Sciences and Engineering Research Council of Canada.

[1] G. H. Flammer, "Ultrasonic Measurement of Suspended Sediment," U.S. Geol. Surv. Bull. **1141**-A, 1962.

[2] M. C. Davis, "Coal slurry diagnostics by ultrasound transmission," J. Acoust. Soc. Am. **64**(2), 406–411 (1978).

[3] R. A. Sigelmann and J. M. Reid, "Analysis and measurement of ultrasound backscattering from an ensemble of scatterers excited by sine-wave bursts," J. Acoust. Soc. Am. **53**(5), 1351–1355, 1973.

[4] C. F. Greenlaw and R. K. Johnson, "Physical and acoustical properties of zooplankton", J. Acoust. Soc. Am. **72**, 1706–1710 (1982).

[5] R. A. Young, J. T. Merrill, T. L. Clarke, and J. R. Proni, "Acoustic profiling of suspended sediments in the marine bottom boundary layer," Geophy. Res. Lett. **9**, 175–178 (1982).

[6] A. E. Hay, "On the remote acoustic detection of suspended sediment at long wavelengths," J. Geophys. Res. **88**, 7525–7542 (1983); J. F. Lynch, "Theoretical analysis of ABSS data for HEBBLE," Mar. Geol. **66**, 277–289 (1985).

[7] A. S. Schaafsma and W. J. G. J. der Kinderen, "Ultrasonic Instruments for the Continuous Measurement of Suspended Sand Transport," in *Proceedings of the IAHR Symposium on Measuring Techniques in Hydraulic Research*, edited by A. C. E. Wessels (Balkema, Rotterdam, 1986).

[8] D. V. Holliday, "Acoustic determination of suspended particle size spectra," Coastal Sediments '87, 260–271 (1987).

[9] D. M. Hanes, C. E. Vincent, D. A. Huntley, and T. L. Clarke, "Acoustic Measurements of Suspended Sand Concentration in the C^2S^2 Experiment at Stanhope Lane, Prince Edward Island," Mar. Geol. **81**, 185–196 (1988).

[10] C. A. Vincent and M. O. Green, "Field measurements of the suspended sand concentration profiles and fluxes and of the resuspension coefficient γ_0 over a rippled bed," J. Geophys. Res. **95**, 11591–11601 (1990).

[11] J. F. Lynch, T. F. Gross, B. H. Brumley, and R. A. Filyo, "Sediment concentration profiling in HEBBLE using a 1-MHz acoustic backscatter system," Mar. Geol. **99**, 361–385 (1991).

[12] P. D. Thorne, C. E. Vincent, P. J. Hardcastle, S. Rehman, and N. Pearson, "Measuring suspended sediment concentrations using acoustic backscatter devices," Mar. Geol. **98**, 7–16 (1991).

[13] A. E. Hay and Jinyu Sheng, "Vertical profiles of suspended sand concentration and size from multifrequency acoustic backscatter," J. Geophys. Res. **97**(C10), 15,661–15,677 (1992).

[14] L. R. Dragonette, R. H. Vogt, L. Flax, and W. G. Neubauer, "Acoustic reflection from elastic spheres and rigid spheres and spheriods. II. Transient analysis," J. Acoust. Soc. Am. **55**, 1130–1137 (1974).

[15] D. Chu, T. Stanton, and P. H. Wiebe, "Frequency dependence of sound backscattering from live zooplankton," ICES J. Mar. Sci. **49**, 97–106 (1992).

[16] A. E. Hay, "Sound scattering from a particle-laden, turbulent jet," J. Acoust. Soc. Am. **90**, 2055–2074 (1991).

[17] V. K. Varadan, Y. Ma, and V. A. Varadan, "A multiple scattering theory for elastic wave propagation in discrete random media," J. Acoust. Soc. Am. **77**, 375–385 (1985).

[18] J. J. Faran, Jr., "Sound scattering by solid cylinders and spheres," J. Acoust. Soc. Am. **23**, 405–418 (1951).

[19] R. Hickling, "Analysis of echoes from a solid elastic sphere in water," J. Acoust. Soc. Am. **34**, 1582–1592 (1962).

[20] A. E. Hay and D. G. Mercer, "On the theory of sound scattering and viscous absorption in aqueous suspensions at medium and short wavelengths," J. Acoust. Soc. Am. **78**, 1761–1771 (1985).

[21] J. M. Reid, "Self-reciprocity calibration of echo-ranging transducers," J. Acoust. Soc. Am. **55**, 862–868 (1974).

[22] A. Crawford, "A Comparison of Two Inversion Methods for Determination of Sand Concentration and Size from Multifrequency Acoustic Backscatter," M.Sc. thesis, Memorial University of Newfoundland, 114 pp. (1991).

[23] A. Crawford and A. E. Hay, "Determining suspended sand size and concentration from multifrequency acoustic backscatter," J. Acoust. Soc. Am. (accepted).

[24] F. H. Fisher, and V. P. Simmons, "Sound absorption in sea water," J. Acoust. Soc. Am. **63**, 558–564 (1977).

[25] C. He, "Broadband measurements of the acoustic backscatter cross section of sand particles in suspension," M.Sc. thesis, Memorial University of Newfoundland, 109 pp. (1991).

[26] C. He and A. E. Hay, "Near-field characteristics of circular piston radiators with simple support," J. Acoust. Soc. Am. **94**, 554–561 (1993).

[27] T. Hasegawa, N. Inoue, and K. Matsuzawa, "A new rigorous solution for the velocity potential of a circular piston," J. Acoust. Soc. Am. **74**, 1044–1047 (1983).

[28] C. S. Clay, and H. Medwin, *Acoustical Oceanography: Principles and Applications* (Wiley, New York, 1977).

[29] S. P. Clarke, "Handbook of Physical Constants," Geol. Soc. Am. Mem. **97**, revised edition, 197–201 (1966).